Structure and Friction of Stearic Acid and Oleic Acid Films Adsorbed on Iron Oxide Surfaces in Squalane

Structure and friction of stearic acid and oleic acid films adsorbed on iron-oxide surfaces in squalane

Michael Doig,[†] Chris P. Warrens,[‡] and Philip J. Camp[*,†]

School of Chemistry, University of Edinburgh, West Mains Road, Edinburgh EH9 3JJ, Scotland, and BP International Limited, Research and Technology Fuels and Lubricants, Technology Centre, Whitchurch Hill, Pangbourne, Reading RG8 7QR, England

E-mail: philip.camp@ed.ac.uk

[*]To whom correspondence should be addressed
[†]University of Edinburgh
[‡]BP International Limited

Abstract

The structure and friction of fatty-acid surfactant films adsorbed on iron-oxide surfaces lubricated by squalane are examined using large-scale molecular dynamics simulations. The structures of stearic-acid and oleic-acid films under static and shear conditions, and at various surface coverages, are described in detail, and the effects of unsaturation in the tail group are highlighted. At high surface coverage, the measured properties of stearic-acid and oleic-acid films are seen to be very similar. At low and intermediate surface coverages, the presence of a double bond, as in oleic acid, is seen to give rise to less penetration of lubricant in to the surfactant film, and less layering of the lubricant near to the film. The kinetic friction coefficient is measured as a function of shear rate within the hydrodynamic (high shear rate) lubrication regime. Lubricant penetration and layering is observed to be correlated with friction coefficient. The friction coefficient with oleic acid depends only weakly on surface coverage, while stearic acid admits more lubricant penetration, and its friction coefficient increases significantly with decreasing surface coverage. Connections between film structure and friction are discussed.

1 Introduction

The adsorption of surfactant molecules on to solid surfaces can be used to control the chemical and physical properties of materials. The range of applications is vast, from dispersing solid particles in colloidal suspensions, through to altering the tribological properties of a solid surface. One of the most important applications, from an economical point of view, is the adsorption of surfactant molecules on to lubricated metal, metal-oxide, and glassy inorganic surfaces in automotive engines, in order to minimize chemical corrosion and mechanical wear, and to control friction. In order to understand how chemistry controls the performance of a surfactant in this application, it is necessary to obtain a clear picture of the structure of the surface-adsorbed film and its modification of the interface between the inorganic surface and the hydrocarbon lubricant. Current commercial surfactants are subject to strict confidentiality agreements, but in general terms they are often relatively simple, amphiphilic molecules, each possessing a polar head group and an aliphatic tail. The binding of the molecules to the surface must be neither too strong (in which case surface corrosion can occur) nor too weak (in which case, the surface film is too fragile). Canonical surfactant molecules include long-chain carboxylic acids, with aliphatic tails consisting of 16 to 18 carbons. Detailed structural information on surface-adsorbed films at the solid-oil interface can be gleaned from techniques such as sum frequency spectroscopy (SFS) and polarized neutron reflectometry (PNR). For example, PNR was used to investigate the structure of palmitic acid [hexadecanoic acid, $CH_3(CH_2)_{14}COOH$] adsorbed on to iron-oxide surfaces from hexadecane.[1] At the bulk-solution concentrations studied, palmitic acid forms a dense tilted monolayer with an apparent thickness of 16 Å. The existence of a second, diffuse layer was assumed in order to fit the reflectometry results; this layer had a thickness of 35-45 Å, depending on solution concentration. Stearic acid [octadecanoic acid, $CH_3(CH_2)_{16}COOH$] and oleic acid [(9Z)-octadec-9-enoic acid, $CH_3(CH_2)_7(CH)_2(CH_2)_7COOH$] have been widely studied in a variety of tribological contexts. The effects of unsaturation on the frictional properties of stearic acid and oleic acid on mica lubricated with *n*-hexadecane have been examined experimentally using surface-force apparatus.[2] Both fatty acids form disordered monolayers on mica over adsorption times of up to 1 day. For

surfaces separated by $H = 50$ Å films consisting of fatty acid and any co-adsorbed lubricant, the friction coefficient of stearic acid at a sliding velocity of $v_s = 4$ μm s^{-1} (and nominal shear rate $\dot{\gamma} = v_s/H = 800$ s^{-1}) was found to be lower than that of oleic acid. Under high loads (in excess of 3.5 MPa) the fatty acid molecules were removed from the surface under sliding, and the measured friction coefficient approached that of pure *n*-hexadecane. In recent work, it has been shown that in the boundary lubrication regime (high load, low sliding velocity), the presence of stearic acid adsorbed on steel surfaces results in a friction coefficient that increases with sliding velocity, while the presence of oleic acid leads to the opposite trend.[3] The presence of the *trans* isomer of oleic acid (elaidic acid) gives the same trend as stearic acid, showing that the structure of the adsorbed film (which is dictated by molecular structure) can have a qualitative effect on friction. The frictional and anti-wear effects of adsorbed stearic and oleic acids have been examined for a variety of surfaces, including steel,[4] TiO_2 crystallites,[5,6] and copper/copper sulfide.[7]

The aim of the current work is to elucidate the microscopic structure of stearic-acid and oleic-acid films adsorbed on to iron-oxide surfaces from a model base oil (squalane), to calculate the kinetic friction coefficient as a function of sliding velocity, and to explore whether any links can be made between the structure and friction. These particular fatty acids allow the effects of unsaturation on structure and friction to be isolated, while iron oxide and squalane are good representatives for components of combustion engines. For the most part, detailed experimental studies of friction between surfaces are limited to high loads and low sliding velocities, i.e., the boundary friction regime. In some critical areas of a combustion engine, the loads and sliding velocities are very high, and pressures up to 1 GPa and shear rates up to 10^9 s^{-1} are possible. In this so-called hydrodynamic lubrication regime, atomistically detailed molecular simulations can provide unique insights on the structure and frictional properties of adsorbed surfactant films. Examples of systems studied using atomistic molecular-dynamics (MD) simulations include generic models of surfaces, lubricant, and friction modifiers,[8] molybdenum sulfide,[9,10] confined polymers and hydrocarbons,[11,12] zinc dithiophosphate in hexadecane between iron-oxide surfaces,[13] and various silane monolayers between silica surfaces.[14–16] More idealized, coarse-grained models have been

studied with a view to understanding the fundamentals of sliding friction,[17–23] and the friction of complex fluids such as polymers, polymer brushes, etc.[24–38] Some important studies of MD methodology have also appeared in the literature, including how to simulate sliding friction under conditions of constant lubricant chemical potential,[39] and the pros and cons of simulating sliding friction under either constant surface separation or constant load.[16,40]

The results from the current work provide insights on the links between structure and friction. Relevant experimental measurements are not yet available for comparison with the simulation results. Nonetheless, a preliminary comparison of simulation results with PNR and SFS measurements for fatty amines on iron-oxide surfaces in oil[41] shows excellent agreement in terms of density profiles and molecular tilt angles, validating the simulation approach.[42] In addition to providing molecular-scale insight on the properties of adsorbed fatty acids at the iron oxide-squalane interface, the current simulation results allow an investigation of some generic properties of lubricant films under high-shear conditions, such as the dependence of friction coefficient on shear rate, and the phenomenon of shear thinning.

The rest of this article is organized as follows. The simulation model and methods are detailed in Section 2. The results are presented in Section 3, arranged in terms of structure under static conditions (Section 3.1), structure under shear conditions (Section 3.2), and friction coefficients (Section 3.3). Conclusions are presented in Section 4.

2 Model and methods

Classical MD simulations were performed using LAMMPS.[43,44] The atomic coordinates for the (100) surface of iron (III) oxide (hematite, α-Fe_2O_3)[45] were used to produce a slab containing 2400 atoms, with lateral (xy) dimensions of 55.1 Å $\times$ 50.4 Å, and a thickness of approximately 10 Å. Two such slabs were used to confine a lubricant layer of squalane, and surfactant molecules (either stearic acid or oleic acid) were adsorbed on to the interior surfaces of the slabs. The system was accommodated in a cuboidal simulation box with periodic boundary conditions applied in the

x and y directions. Three surface coverages were considered, each with a different number of lubricant molecules, but with a similar total number of atoms ($N \simeq 27\,000$ atoms including the surface atoms): 72 surfactants on each interior surface (giving a surface coverage $\Gamma = 2.59$ nm^{-2}) and 168 squalanes; 36 surfactants ($\Gamma = 1.30$ nm^{-2}) and 192 squalanes; 16 surfactants ($\Gamma = 0.58$ nm^{-2}) and 240 squalanes. In each case, the average surface-surface separation (measured in the z direction between the innermost layer of atoms on each iron-oxide surface) was in the region of $H_z = 75$-90 Å, which was large enough so that no significant lubricant structuring was evident in the middle of the fluid layer. Some representative simulation snapshots are shown in Figure 1. In the following, squalane will be referred to as the 'lubricant'. In real systems, the amount of 'lubricant' between surfaces can be very small – particularly in the boundary lubrication regime – and hence the distinction between 'lubricant' and adsorbed 'surfactant' becomes blurred. In the simulated systems, this distinction remains clear and we use the terms 'lubricant' and 'surfactant' to refer to the squalane and stearic acid/oleic acid, respectively.

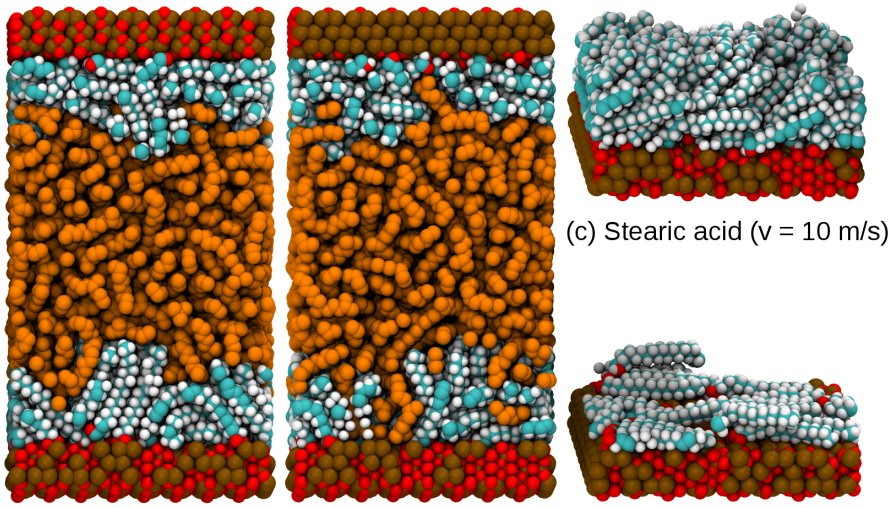

Figure 1: Simulation snapshots of the surfactant film, with and without lubricant. (a) Stearic acid at $\Gamma = 2.59$ nm^{-2} under static conditions. (b) Oleic acid at $\Gamma = 2.59$ nm^{-2} under static conditions. (c) A single stearic acid film at $\Gamma = 2.59$ nm^{-2} with sliding velocity $v_s = 10$ m s^{-1} (lubricant not shown). (d) A single stearic acid film at $\Gamma = 0.58$ nm^{-2} with sliding velocity $v_s = 10$ m s^{-1}, showing the 'piling up' effect (lubricant not shown). These figures were prepared using VMD.[46]

Interactions involving surfactant and lubricant molecules were described using the DREID-

ING force field,[47] which discriminates between the hybridization states of atoms through bonding constraints, and hence can represent the differences in interactions involving stearic acid and oleic acid. The surfactant molecules were taken to be in the protonated (electrically neutral) form, which should be favored in a low-polarity solvent. Partial charges on surfactant head-group atoms were determined using Gaussian 03[48] at the B3LYP level with the 6-311+G(d,p) basis set, and these values were used in combination with the non-electrostatic interactions from the DREIDING force field. The atom partial charges were found to be the same for both stearic acid and oleic acid: hydroxyl H $+0.46$ e; hydroxyl O -0.65 e; carbonyl C (C1) $+0.73$ e; carbonyl O -0.52 e; alkyl C (C2) -0.05 e; alkyl C (C3) $+0.03$ e. All other surfactant atoms had zero partial charges. The iron-oxide surface interactions were represented by the Lennard-Jones-type potential developed by Berro *et al.*[13] In particular, the partial charges on the surface atoms were $+0.771$ e on Fe and -0.514 e on O. The surface atoms were restrained in the prescribed crystal structure by harmonic bonds between neighboring atoms within 3 Å of one another: the force constant was chosen to be 130 kcal mol^{-1} Å^{-2}, which kept the surface structure rigid, but did not adversely affect thermostatting (see below). All LJ-type interactions were cut-off at 10 Å, and cross interactions were evaluated using the Lorentz-Berthelot mixing rules. Electrostatic interactions were evaluated using a slab implementation of the particle-particle particle-mesh algorithm.

The MD equations of motion were integrated using the velocity-Verlet algorithm with an integration time-step of 1 fs. A Nosé-Hoover thermostat was applied to keep a constant temperature $T = 298$ K. Pressure was controlled by applying a normal load ($P_{zz} = 1000$ atm) to the outermost layer of atoms in the upper slab, keeping the z coordinates of the outermost layer of atoms in the lower slab fixed in space.[49] Calculations of the stress tensor showed that the hydrostatic pressure within the fluid film was equal to its target value. Under shear conditions, the outermost layer of atoms in each slab was given a constant sliding velocity of $\pm v_s/2$ in the x direction. The values of v_s were 0.625, 1.250, 2.500, 5.000, 10.000, and 20.000 m s^{-1}, and the thermostat was then only applied in the y direction (perpendicular to the xz shear plane) so as not to perturb the steady-state velocity profile $v_x(z)$. The kinetic friction coefficient μ can be obtained using the

extended Amontons-Coulomb law $F_{\mathrm{L}} = F_0 + \mu F_{\mathrm{N}}$, where F_{L} and F_{N} are, respectively, the average total lateral and normal forces acting on the outermost layer of atoms in each slab, and F_0 is the load-independent, Derjaguin offset representing adhesive surface forces. In the present case, because the normal force (load) is so high, the approximation $F_{\mathrm{L}}/F_{\mathrm{N}} = F_0/F_{\mathrm{N}} + \mu \simeq \mu$ is very accurate and computationally expedient. It was checked for some test cases that a linear fit of F_{L} as a function of F_{N} gives an insignificant value of F_0 and the same result for μ within the statistical uncertainties. In general, the formula $\mu \simeq F_{\mathrm{L}}/F_{\mathrm{N}}$ is appropriate for the cases of non-adhesive surfaces (small F_0) and any surfaces under high applied loads (large F_{N}).[19]

The simulation setup consisted of placing surfactant molecules close to, but not directly on, the interior surfaces of two well-separated slabs ($H_z \simeq 200$ Å), and introducing several perfectly ordered layers of squalane molecules in between. The system was then allowed to equilibrate and compress slowly under the applied load. Equilibration runs were typically in the range of 20-40 ns, and production runs were 20 ns. All calculations were run on BP's High Performance Computing facility in Houston, USA. Even with such resources, the calculations were demanding: a typical 20 ns simulation took around 5 days running in parallel on 60 Nehalem or Westmere cores.

3 Results and discussion

Some simulation snapshots are shown in Figure 1, for stearic acid and oleic acid at high surface coverage and under static conditions, and stearic acid under shear conditions at high and low surface coverages. In what follows, some properties are expressed as functions of the distance from the surface, denoted by z. This is taken as the distance from the innermost layer of atoms on each slab.

3.1 Structure under static conditions

The structure of the adsorbed surfactant film under static conditions is considered first. Figure 2 shows the atomic mass-density profiles $\rho(z)$ resolved in to surfactant and lubricant contributions.

Results are shown for stearic acid and oleic acid, and under three different surface coverages Γ. The surfactant film gets thicker with increasing surface coverages: the tail of $\rho(z)$ extends further in to the lubricant. Broadly speaking, the surfactant forms a film that extends up to about 20 Å from the surface, and there is no evidence for multilayer formation. At the highest surface coverage ($\Gamma = 2.59$ nm^{-2}) the lubricant near the surfactant layer shows only a small degree of modulation that signals layering. With decreasing surface coverage, the lubricant develops more structure, reflecting the increasing influence of the hard iron-oxide surface. In essence, the surfactant film is 'soft' and leads to a blurring of the interface between surface and lubricant.

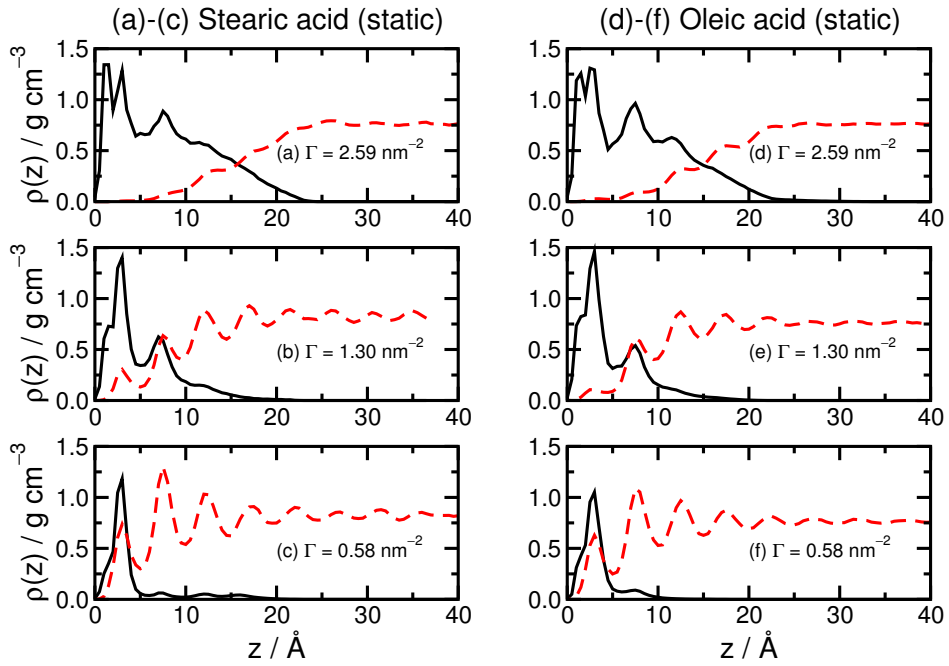

Figure 2: Atomic mass-density profiles $\rho(z)$ of surfactant and lubricant molecules, as functions of the distance from the surface z, under static conditions. Panels (a)-(c) and (d)-(f) show the results for stearic acid and oleic acid, respectively, at the indicated values of surface coverage Γ. Black solid lines: surfactant atoms. Red dashed lines: lubricant atoms.

Ostensibly, the profiles for stearic acid and oleic acid are very similar, but there is a subtle and important difference at the lowest surface coverage ($\Gamma = 0.58$ nm^{-2}): the squalane appears to penetrate further in to the stearic-acid film than in to the oleic-acid film. This is signaled by the first two peak heights in the squalane density profile being greater with stearic acid than with oleic acid. An associated feature is that the stearic-acid density profile has a small tail that extends further in

to the lubricant, while the backbone atoms of oleic acid form only two 'adlayers'. The difference in film structure between stearic and oleic acids can be highlighted by calculating the center-of-mass, z_{COM}, of the surfactant molecules within a surface film. For a given surface coverage, a more compact surfactant film will give a smaller value of z_{COM}. The results are shown in Table 1. Except for the highest surface coverage, stearic acid gives a higher value of z_{COM} than does oleic acid, showing that the stearic-acid film is more diffuse, i.e., the lubricant penetrates further in to the film and leads to swelling. At the highest surface coverage, the packings of stearic acid and oleic acid should be similar. At low and intermediate surface coverages, oleic acid forms a more compact film that admits less lubricant penetration. Unsaturated molecules usually pack less well in the bulk solid phase, leading to a reduction in melting point as compared with saturated molecules, but for an adsorbed monolayer in intimate contact with liquid-phase squalane, this structure-property relationship is not expected to carry over.

Table 1: Properties of systems with stearic-acid and oleic-acid films at surface coverage Γ: center-of-mass distance z_{COM} of the surfactant molecules within a film under static conditions; fit parameters μ_0 and $\dot{\gamma}_0$ of eq 4 describing the shear-rate dependence of the kinetic friction coefficient.

Surfactant	Γ/nm^{-2}	$z_{\mathrm{COM}}/\mathrm{\AA}$	μ_0	$\dot{\gamma}/10^6\ \mathrm{s}^{-1}$
Stearic acid	0.58	3.8	0.0489 ± 0.0031	1.21 ± 0.45
Stearic acid	1.30	4.9	0.0586 ± 0.0018	2.24 ± 0.37
Stearic acid	2.59	7.5	0.0693 ± 0.0031	22.5 ± 3.1
Oleic acid	0.58	2.9	0.0659 ± 0.0013	27.2 ± 1.6
Oleic acid	1.30	4.4	0.0635 ± 0.0030	21.4 ± 3.3
Oleic acid	2.59	7.5	0.0635 ± 0.0028	21.3 ± 3.0

The thickness of the film can also be characterized by the distances of certain backbone atoms from the surface. The distance of the terminal carbon (C18) from the surface could reasonably be taken to represent the height of the film, denoted by h. The height probability distribution $p(h)$ in Figure 3 shows the following features. At high surface coverage ($\Gamma = 2.59\ \mathrm{nm}^{-2}$) the height distribution is rather broad, but with a peak in the region of $h = 20$ Å. At low surface coverage ($\Gamma = 0.58\ \mathrm{nm}^{-2}$) $p(h)$ is dominated by two peaks at $h \simeq 1$ Å and 4 Å. At intermediate surface coverage ($\Gamma = 1.30\ \mathrm{nm}^{-2}$) $p(h)$ is a superposition of the distributions at the two extremes. These results show that at high surface coverage, the surfactant molecules are primarily pointing upwards,

due to the packing of the molecules. At low surface coverage, the molecules lie either completely flat so that the terminal carbon atoms are on the surface, or somewhat upright. These basic trends are illustrated by the simulation snapshots shown in Figure 1. There are only small differences between stearic acid and oleic acid. Stearic acid shows a long tail in $p(h)$, as observed previously in the density distribution $\rho(z)$ in Figure 2. The relative weights of the 1 Å and 4 Å peaks in oleic acid are shifted in favor of the longer-distance peak, due to the more rigid backbone arising from the presence of the unsaturated C9-C10 bond.

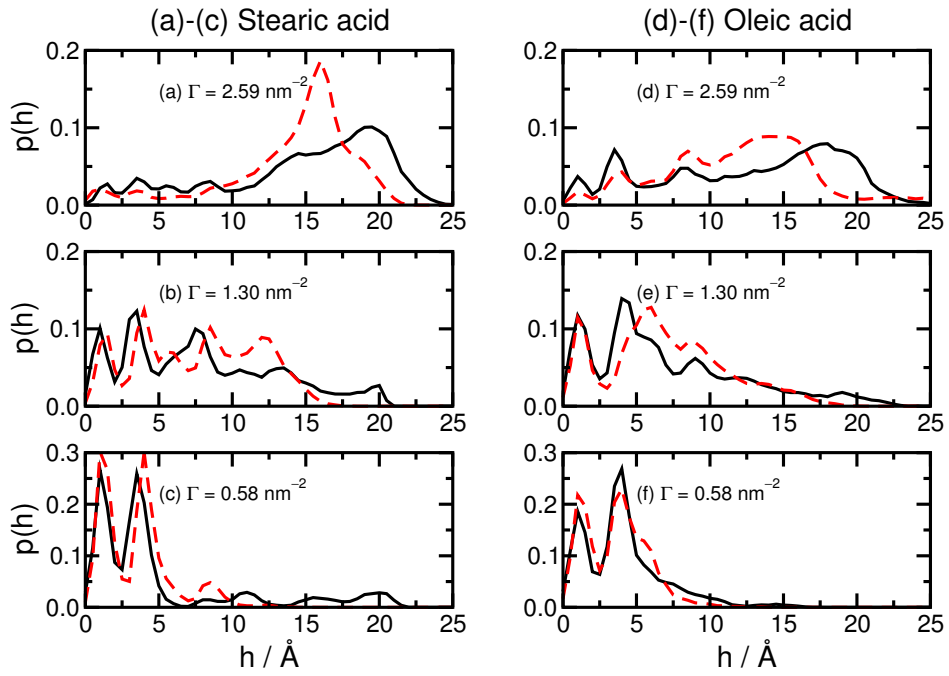

Figure 3: Probability distribution $p(h)$ of the film height h, defined as the distance of the terminal carbon atom (C18) from the surface. Panels (a)-(c) and (d)-(f) show the results for stearic acid and oleic acid, respectively, at the indicated values of surface coverage Γ. Black solid lines: static conditions. Red dashed lines: shear conditions with $v_s = 10$ m s^{-1}.

Of particular interest in this work is the effect of the double bond between carbons C9 and C10. Figure 4 shows the probability distribution $p(z)$ of the distance z of the C9 atom from the surface. The distributions are qualitatively similar to those for the C18 atom, except that at high surface coverage, the main peak is at $h \simeq 10$ Å, i.e., half-way along the chain. There is a difference in $p(z)$ between stearic acid and oleic acid at $\Gamma = 1.30$ nm^{-2}, with the oleic acid showing a broader distribution up to a higher maximum distance of around 15 Å, as opposed to 13 Å for stearic acid.

This is presumably due to the stiffer backbone of the oleic acid molecule.

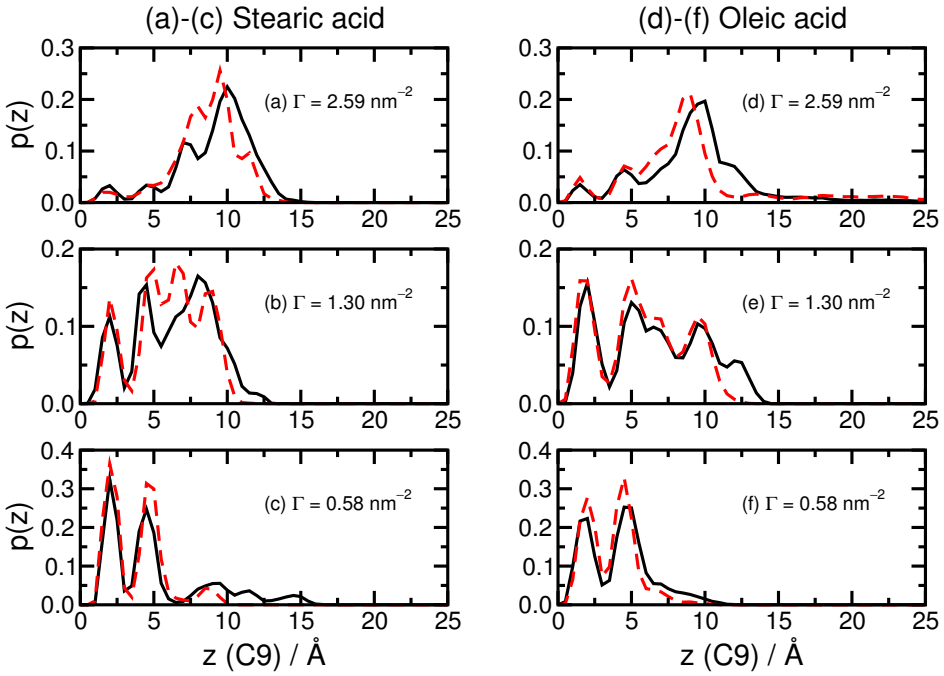

Figure 4: Probability distribution $p(z)$ of the distance z of the C9 atom from the surface. Panels (a)-(c) and (d)-(f) show the results for stearic acid and oleic acid, respectively, at the indicated values of surface coverage Γ. Black solid lines: static conditions. Red dashed lines: shear conditions with $v_s = 10$ m s^{-1}.

Figure 5 shows the distribution of the angle θ between a vector from the carboxyl C1 atom to the C9 atom, and the surface plane. At high surface coverage, stearic acid and oleic acid show broad 'upright-molecule' peaks centered on $\theta \simeq 45°$ and $\theta \simeq 60°$, respectively, and small 'flat-molecule' peaks in the region of $\theta < 15°$. The increase in upright angle with the introduction of the C9-C10 double bond is likely to be connected with the increase in molecular rigidity. As the surface coverage is reduced, molecules are more likely to lie flat on the surface, and less likely to remain upright. This was shown earlier in the atom-height distributions $p(h)$ and $p(z)$ (Figures 3 and 4, respectively).

The structure within the surfactant film was examined further using the two-dimensional radial distribution function (RDF), $g(r)$, calculated separately for the head-group carbon (C1), one of the central carbons (C9), and the terminal carbon (C18). The particle coordinates were projected on to the surface (xy) plane, and the RDF was calculated in the usual way.[50] Figure 6 shows the results.

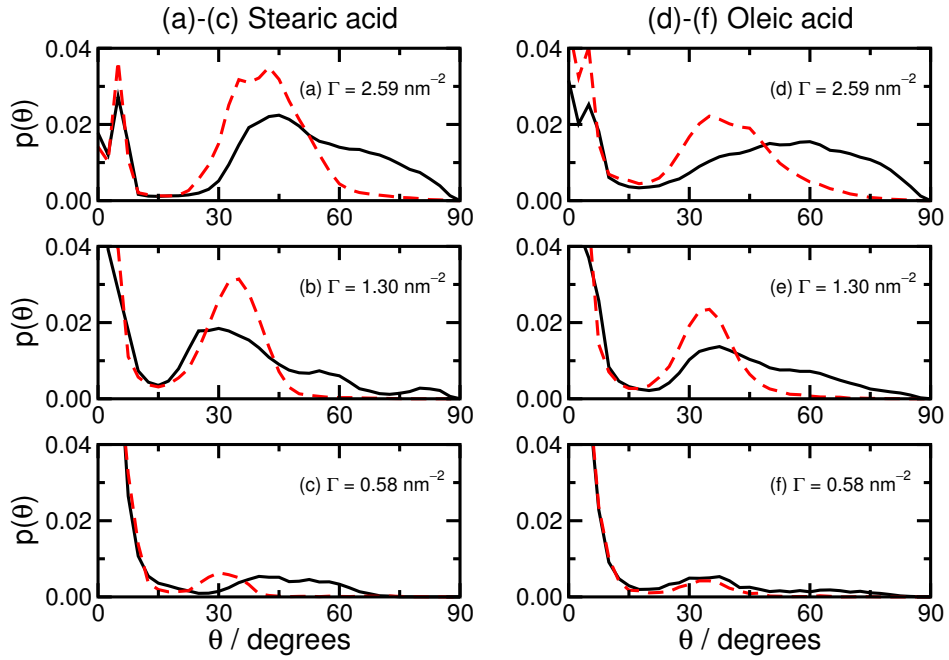

Figure 5: Probability distribution $p(\theta)$ of the angle θ between the surface plane and the vector joining the carboxylic carbon and the terminal carbon atom. Panels (a)-(c) and (d)-(f) show the results for stearic acid and oleic acid, respectively, at the indicated values of surface coverage Γ. Black solid lines: static conditions. Red dashed lines: shear conditions with $v_s = 10$ m s^{-1}.

At each surface coverage, the C1 RDF shows the most structure, with the major peaks occurring at multiplies of $r = 5$ Å, which is the unit-cell dimension of the hematite surface.[45] This shows that the surface dictates the head-group packing in the surfactant film. The C9 and C18 RDFs show progressively less structure as the influence of the surface on the aliphatic tails decreases. At high surface coverage ($\Gamma = 2.59$ nm^{-2}), there is very little difference between the structures of the stearic-acid and oleic-acid films. At intermediate and low surface coverages ($\Gamma = 1.30$ and 0.58 nm^{-2}, respectively) the C9 and C18 RDFs for stearic acid show more structure than those for oleic acid. This is consistent with the observation that there is more lubricant penetration in to the stearic-acid film; the interdigitation of the squalane molecules with the stearic-acid molecules could help retain some structuring of the C9 and C18 carbons in the plane of the surface.

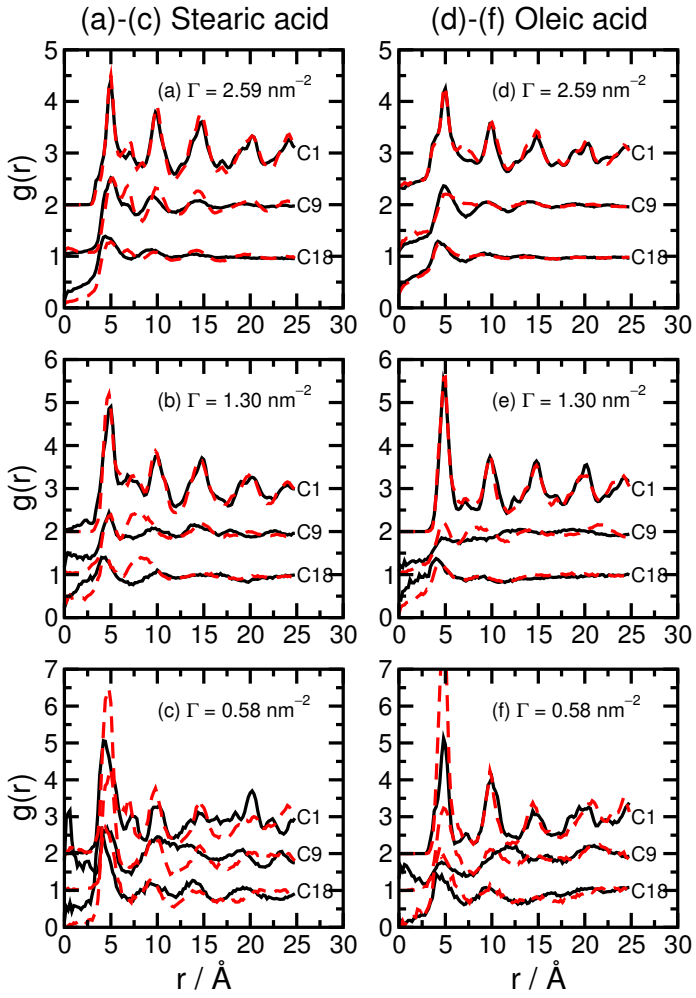

Figure 6: Two-dimensional radial distribution functions, $g(r)$, for C1, C9, and C18 carbons in the surface (xy) plane; the C9 and C1 functions are shifted up by 1 and 2 units, respectively. Panels (a)-(c) and (d)-(f) show the results for stearic acid and oleic acid, respectively, at the indicated values of surface coverage Γ. Black solid lines: static conditions. Red dashed lines: shear conditions with $v_s = 10$ m s^{-1}.

3.2 Structure under shear conditions

Simulation timescales limit the range of sliding velocities and shear rates that can be surveyed. In this work, sliding velocities in the range $v_s = 0.625$-20 m s^{-1} have been studied. With average surface-surface separations in the range $H_z = 75$-90 Å, these velocities correspond to nominal shear rates $\dot{\gamma} = v_s/H_z$ in the range 7×10^7-3×10^9 s^{-1}. The effective shear rate in the middle of the fluid layer is given by $\dot{\gamma}_{\text{eff}} = (\partial v_x/\partial z)_y$ and will, in general, be different from $\dot{\gamma}$ due to stick or slip at the boundaries. Stick or slip can be represented by a length parameter λ defined by $\dot{\gamma}_{\text{eff}} = v_s/(H_z + \lambda)$,

where $\lambda > 0$ for slip and $\lambda < 0$ for stick at the liquid-solid boundary. Fitting the linear portion of $v_x(z)$ in the middle of the liquid layer and extracting $\dot{\gamma}_{\rm eff}$ yields λ. Examples for stearic acid and oleic acid with $\Gamma = 2.59$ nm^{-2} and $v_{\rm s} = 20$ m s^{-1} are shown in Figure 7. The fits give a stick length of $\lambda \simeq -25$ Å in each case. $\lambda < 0$ because the surfactant film is strongly anchored to the surface, and so the thickness of the flowing lubricant layer is less than H_z. Taking in to account that there is one surfactant film on each surface, the effective dynamical thickness of each film is $|\lambda|/2 \simeq$ 12-13 Å. The slip planes are located at $z = -\lambda/2$ and $z = H_z + \lambda/2$, and these are indicated by the vertical dotted lines in Figure 7. It was not possible to obtain reliable stick lengths at lower sliding velocities; while values of λ are of order 10% of the liquid-layer thickness, the statistical errors approach 100%. Given that the difference between the nominal and effective shear rates is only of order 10% (and with a large statistical uncertainty), the nominal shear rate will be used in what follows.

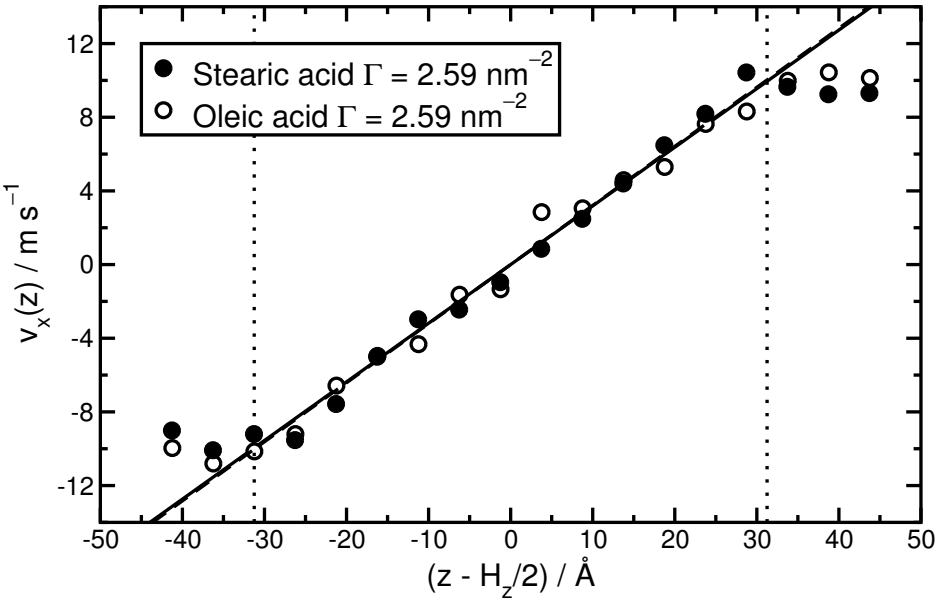

Figure 7: Velocity profiles $v_x(z)$ for stearic acid (filled symbols) and oleic acid (open symbols) with sliding velocity $v_{\rm s} = 20$ m s^{-1}. Straight lines have been fitted to the linear region 20 Å either side of the mid-point of the liquid layer $z = H_z/2$, where $H_z \simeq 87.5$ Å for both systems. The gradient is the effective shear rate $\dot{\gamma}_{\rm eff} = v_{\rm s}/(H_z + \lambda)$. The fits yield for stearic acid $\dot{\gamma}_{\rm eff} = (3.18 \pm 0.14) \times 10^9$ s^{-1} and $\lambda = (-25.1 \pm 5.0)$ Å (solid line) and for oleic acid $\dot{\gamma}_{\rm eff} = (3.21 \pm 0.26) \times 10^9$ s^{-1} and $\lambda = (-24.7 \pm 2.3)$ Å (dashed line); the two lines are almost indistinguishable on the plot. The apparent slip planes at $z = -\lambda/2$ and $z = H_z + \lambda/2$ are indicated by vertical dotted lines.

Figure 8 shows the mass-density profiles of the surfactant and lubricant at $v_s = 10$ m s^{-1}. Surprisingly, they differ only slightly from those under static conditions (Figure 2). Looking at high surface coverage ($\Gamma = 2.59$ nm^{-2}) the surfactant-film thickness (~ 15 Å) compares well with the dynamical film thickness (12-13 Å) obtained from the stick length.

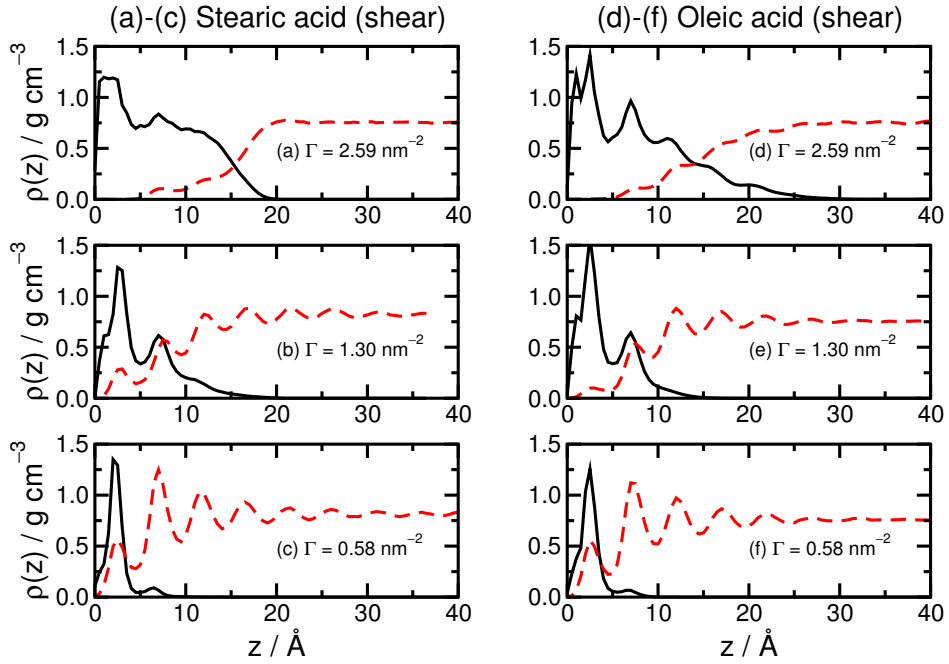

Figure 8: Mass-density profiles $\rho(z)$ of the backbone atoms (all atoms except H) in the surfactant and lubricant molecules, as a function of the distance from the surface z, under shear conditions with $v_s = 10$ m s^{-1}. Panels (a)-(c) and (d)-(f) show the results for stearic acid and oleic acid, respectively, at the indicated values of surface coverage Γ. Black solid lines: surfactant atoms. Red dashed lines: lubricant atoms.

One might anticipate that the surfactant molecules tilt under the application of shear, and this is confirmed in Figure 5: essentially, shear leads to an increasing preference for an angle in the range $\theta \simeq$ 30-45°, and a lower probability of having angles close to 90°. At the same time, the molecules will, on average, sample more extended conformations due to being dragged by the neighboring lubricant molecules undergoing shear flow. This is shown explicitly in Figure 9(a), where the root-mean-square end-to-end (C1-C18) distance $\sqrt{\langle R_{ee}^2 \rangle}$ is plotted as a function of shear rate for each surfactant and surface coverage. Oleic acid is 'shorter' than stearic acid due to the presence of the C9-C10 *cis* double bond. The magnitude of the molecular elongation under shear is less sensitive to surface coverage for oleic acid than for stearic acid: oleic acid has an intrinsic

molecular rigidity, whereas the elongation of stearic acid molecules is more strongly influenced by the crowding effects of neighboring adsorbed molecules.

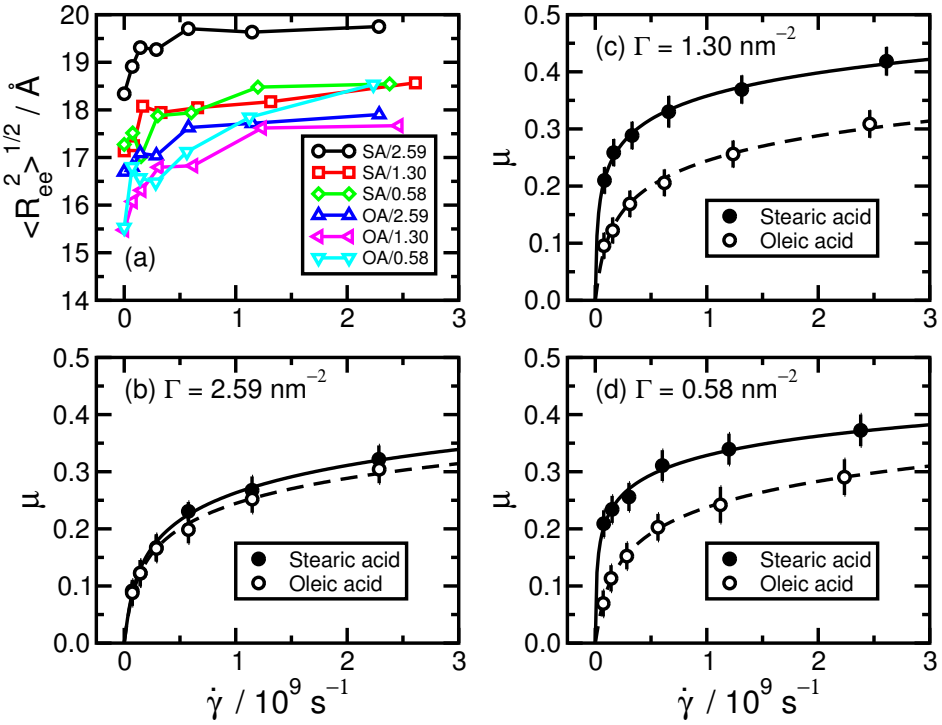

Figure 9: (a) Root-mean-square end-to-end distance (C1-C18) as a function of shear rate $\dot{\gamma}$: SA/2.59, SA/1.30, and SA/0.58 mean stearic acid at $\Gamma = 2.59$, 1.30, and 0.58 nm^{-2}, respectively; OA/2.59, OA/1.30, and OA/0.58 mean oleic acid at $\Gamma = 2.59$, 1.30, and 0.58 nm^{-2}, respectively. (b)-(d) Kinetic friction coefficient μ as a function of shear rate $\dot{\gamma}$. Points: simulation data. Black lines: fits to eq 4. Panels (b), (c), and (d) show the results for stearic acid (filled symbols and solid lines) and oleic acid (open symbols and dashed lines) at coverages of $\Gamma = 2.59$, 1.30, and 0.58 nm^{-2}, respectively.

The net result of molecular tilt and molecular elongation is that the density profiles (and the overall fluid density in the layer) remain practically unaltered. This is not surprising as the applied normal load of $P_{zz} = 1000$ atm is being supported by the fluid film whether it is under shear or not.

Figures 3 and 4 show the height distributions of the C18 and C9 atoms, respectively, under both shear and static conditions. At high surface coverage, the main effect of shear is to shift the C18 peak from about 20 Å to around 15 Å (in good agreement with the dynamical thickness obtained above from the stick length); the shifts are much less significant at lower surface coverages. The effects of shear on the C9 positions are very small, showing that it is the C9-C18 portion of the

molecule that responds most to the applied shear. As noted above, the molecules are tilting over more, but this does not have a large impact on the distributions of C9 or C18 heights (and the density profiles) due to the simultaneous molecular extension.

Figure 6 shows the C1, C9, and C18 two-dimensional RDFs at $v_s = 10$ m s^{-1}. At high surface coverage ($\Gamma = 2.59$ nm^{-2}) the effect of shear is very small, with only a small increase in structure in the C9 RDFs. At intermediate surface coverage ($\Gamma = 1.30$ nm^{-2}) the C1 RDF is practically unchanged by shear, while the C9 and C18 RDFs develop a little more structure. The stearic-acid RDFs show a greater response to shear than the oleic-acid RDFs, presumably due to the inherent molecular rigidity of the unsaturated molecule. At the lowest surface coverage, all of the RDFs signal an increase in structure with the application of shear, due to the shear alignment of the surfactant tails. The primary peak in the C1 RDF of the oleic-acid film shows the greatest increase, which could be correlated with less lubricant penetration: while the head-group ordering in the stearic-acid film may be compromised by interactions with lubricant molecules, the head-group ordering in the oleic-acid film can increase unhindered by lubricant molecules.

3.3 Friction coefficients

The measured friction coefficients μ are plotted as functions of the nominal shear rate $\dot{\gamma} = v_s/H_z$ in Figure 9(b)-(d). The general shear-rate dependence of friction will be discussed first, and then a comparison of stearic acid and oleic acid at different surface coverages will be made.

The friction coefficient increases sub-linearly with shear rate. This has now been observed in simulations many times[19,26,31,32,34–37] and in experiments.[51–55] For the most part, the dependence of frictional forces on sliding velocity has been derived theoretically as being logarithmic,[52–57] while others have tried to fit such a dependence with various power laws.[34,35] The current simulation results are consistent with a logarithmic dependence at high shear rates, which may be rationalized using a simple Eyring-like, activated-hopping argument as follows.[3,32,58] Consider the velocity of a fluid-phase molecule adjacent to a planar surface (xy). In the laboratory frame and

in a direction (say x) parallel with the surface, the average velocity of the molecule will be

$$\langle v_x \rangle = (k_+ - k_-)d \tag{1}$$

where $k_\pm$ are rate constants for hopping over molecular-scale energy barriers in the $+x$ and $-x$ directions, and d is a characteristic distance between barriers. These barriers would arise from processes such as molecules squeezing between neighboring molecules, from one solvation cavity to the next. Under static conditions and in a quiescent fluid, the rates will be equal ($k_\pm = k_0$) and the average velocity will be $\langle v_x \rangle = 0$. Now consider the case of a sliding surface with velocity $+v_s$. The surface does work on the fluid molecule, pushing it over barriers in the $+x$ direction more than in the $-x$ direction, so that in the laboratory frame, $\langle v_x \rangle > 0$. This suggests that the associated hopping rates are

$$k_\pm = k_0 \exp(\pm \mu P_{zz} d^3 / k_B T) = k_0 \exp(\pm \mu / \mu_0) \tag{2}$$

where $\mu P_{zz} d^2 = P_{xz} d^2$ is an estimate of the extra force exerted on the molecule by the surface given a fixed downward pressure P_{zz}, $\mu P_{zz} d^3$ is the corresponding energy, and $\mu_0 = k_B T / P_{zz} d^3$ is a dimensionless number. Given these rates, the average velocity in the laboratory frame is

$$\langle v_x \rangle = 2k_0 d \sinh(\mu / \mu_0) = 2v_0 \sinh(\mu / \mu_0) \tag{3}$$

where $v_0 = k_0 d$ is a characteristic speed. If $\langle v_x \rangle$ is proportional to the sliding velocity v_s and hence the shear rate $\dot{\gamma}$ (assuming little slip or stick at the surface) then $\langle v_x \rangle / v_0$ can be written as $\dot{\gamma}/\dot{\gamma}_0$. With this assumption, solving eq 3 for μ gives

$$\mu = \mu_0 \ln \left[(\dot{\gamma}/2\dot{\gamma}_0) + \sqrt{1 + (\dot{\gamma}/2\dot{\gamma}_0)^2} \right]. \tag{4}$$

At low shear rates $\dot{\gamma}/\dot{\gamma}_0 \ll 1$, $\mu \approx \mu_0 \dot{\gamma}/2\dot{\gamma}_0$, while at high shear rates $\dot{\gamma}/\dot{\gamma}_0 \gg 1$, $\mu \approx \mu_0 \ln(\dot{\gamma}/\dot{\gamma}_0)$, as required. The results in Figure 9(b)-(d) have been fitted with eq 4 and the fit parameters are given in Table 1.

The friction coefficient for each of the surfactants, surface coverages, and shear rates is shown on a universal plot of μ/μ_0 against $\dot{\gamma}/\dot{\gamma}_0$ in Figure 10(a). Excellent collapse of the results on to eq 4 is demonstrated, although it should be pointed out that the restriction to high shear rates precludes a proper examination of the crossover from high-shear conditions to low-shear conditions where $\dot{\gamma}/\dot{\gamma}_0 < 1$. This crossover has been explored with coarse-grained models and excellent data collapse was seen under low-shear conditions.[32] Although it is difficult to associate a 'bulk' viscosity with such systems containing a heterogeneous distribution of surfactant and lubricant, an effective value can be defined by $\eta = P_{xz}/\dot{\gamma} = \mu P_{zz}/\dot{\gamma}$. From eq 4, in the low-shear regime $\dot{\gamma} \to 0$, $\mu/\dot{\gamma} \to \mu_0/2\dot{\gamma}_0$, and so the relative viscosity (compared to its low-shear value) is

$$\frac{\eta}{\eta_0} = \frac{\ln\left[(\dot{\gamma}/2\dot{\gamma}_0) + \sqrt{1+(\dot{\gamma}/2\dot{\gamma}_0)^2}\right]}{(\dot{\gamma}/2\dot{\gamma}_0)}. \tag{5}$$

The plot of η/η_0 against $\dot{\gamma}/\dot{\gamma}_0$ in Figure 10(b) shows that, effectively, the lubricating fluid film undergoes shear thinning. Both bulk squalane and confined squalane films are known to undergo significant shear thinning (reduction of shear viscosity by an order of magnitude) over a comparable range of shear rates.[59,60]

Returning to Figure 9(b)-(d), there are some significant differences between the friction coefficients in systems with stearic acid and oleic acid. In the case of stearic acid, for a given shear rate, the friction coefficient is significantly lower at the highest surface coverage than at lower surface coverages. On the other hand, with oleic acid, the friction coefficient is roughly independent of surface coverage. It is not possible to explain this difference completely, but there are some apparent correlations between the friction coefficient and the structural characteristics of the surfactant and lubricant layers. Recall the density profiles in Figure 2. At the highest surface coverage ($\Gamma = 2.59$ nm^{-2}) the density profiles of the fatty acids are very similar, and indeed the friction coefficients are practically identical. At the two lower surface coverages, the lubricant layer penetrates further in to the stearic-acid film than in to the oleic-acid film; in addition, the oscillations in the lubricant-density profile are of larger amplitude and longer range with stearic acid than with oleic

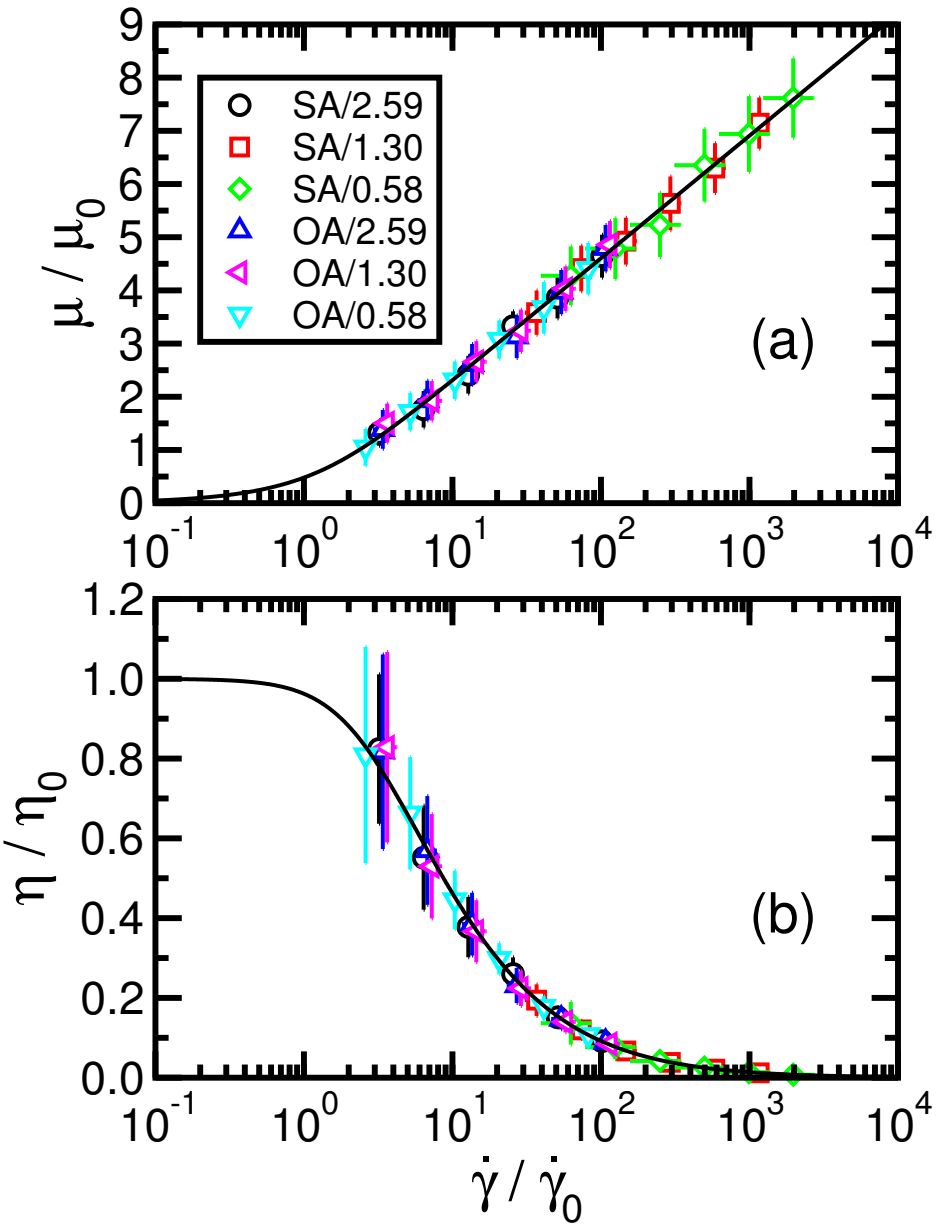

Figure 10: (a) Kinetic friction coefficient μ and (b) effective viscosity η as a function of shear rate $\dot{\gamma}$, plotted in scaled form according to eq 4 and 5, respectively. Points: simulation data; SA/2.59, SA/1.30, and SA/0.58 mean stearic acid at $\Gamma = 2.59$, 1.30, and 0.58 nm^{-2}, respectively; OA/2.59, OA/1.30, and OA/0.58 mean oleic acid at $\Gamma = 2.59$, 1.30, and 0.58 nm^{-2}, respectively. Black lines: (a) eq 4; (b) eq 5.

acid. An additional observation from movies of the simulation trajectories is that the stearic acid molecules tended to sporadically 'pile up' to form structures of greater thickness than an adsorbed monolayer; a typical snapshot of this transient structure is shown in Figure 1(d). All of these observations point to the lubricant having more intimate contact with the iron-oxide surface with

stearic acid than with oleic acid, at low surface coverage, and consequently developing more structure through the lubricant layer. This seems to be correlated with a higher friction coefficient. It appears that surfactant ordering within the plane of the film is not strongly correlated with friction; the relatively small differences between the two-dimensional RDFs of stearic acid and oleic acid are a consequence of lubricant penetration, rather than the cause.

4 Conclusions

In this work, molecular simulations have been used to investigate the structure and friction of a confined fluid film consisting of stearic acid or oleic acid adsorbed on iron-oxide surfaces, lubricated by squalane. The primary aim was to determine the effects of surface coverage, shear rate, and unsaturation in the fatty-acid tail on the observed properties.

Density profiles under static conditions show that at low and intermediate surface coverages, oleic acid forms a more compact surfactant film than does stearic acid, leading to less penetration by the lubricant; the presence of a double bond on the backbone of oleic acid gives it an inherent rigidity, but it does not seem to compromise packing efficiency, which is largely dictated by the hematite structure at the surface coverages considered. At high surface coverage, the film properties of the two fatty acids appear to be very similar. With both fatty acids at low and intermediate surface coverages, orientational distribution functions show that there are significant proportions of molecules lying flat on the surface, as well as pointing out in to the lubricant. The main effect of unsaturation is to make the oleic-acid molecules adopt slightly more upright conformations than stearic-acid molecules at high surface coverage.

Density profiles and two-dimensional radial distribution functions show that the surfactant film does not change significantly under the application of shear. The orientational distribution functions show that the surfactant molecules tilt significantly under shear, while calculations of the end-to-end distance show that the molecules elongate. These two competing effects cancel each other out, leading to the film thickness being insensitive to the applied shear.

The kinetic friction coefficient was measured as a function of shear rate and surface coverage for each fatty acid. Molecular simulations are limited to the hydrodynamic lubrication regime, meaning high shear rates. It was confirmed that the friction coefficient increases logarithmically with shear rate, and a simple theoretical justification was put forward. At the highest surface coverage, the friction coefficients with stearic acid and with oleic acid are very similar for a given shear rate. With decreasing surface coverage, the friction coefficient with oleic acid is almost constant, whereas that with stearic acid increases. These observations can be related to the structural properties of the surfactant film, and in particular, the degree of penetration of the lubricant: a higher degree of lubricant penetration implies more intimate contact with the surface; this gives rise to more structure in the lubricant layer, which is apparently correlated with an increase in friction coefficient. As the surface coverage is reduced, there is more penetration of lubricant in to the stearic-acid film than in to the oleic-acid film, and this correlates well with the behavior of the friction coefficient. Turning this argument around, friction is reduced when there is less lubricant penetration in to the surfactant film, and hence the slip plane is located nearer to the surfactant-lubricant interface than to the surface-surfactant interface. Although it was not possible to measure stick/slip lengths precisely in the simulations, their values are negative implying that the surfactant sticks to the surface, and that the slip occurs near to the surfactant-lubricant interface.

The calculations reported in this work were extremely demanding, and so the study was focused on the specific comparison between stearic acid and oleic acid. There are a large number of other systems of interest that should be studied, in particular to make links with experiment and industrial applications. Mention was already made of a comparison between experimental[41] and simulation results for the structure of fatty amines adsorbed on iron oxide.[42] The effects of specific chemical interactions, stereoisomerism, surface roughness and asperities, surfactant polydispersity, and impurities all deserve to be examined systematically in future work.

Acknowledgement

This research was supported through a CASE studentship for M. D. by BP International Ltd and EPSRC (UK), and by the generous provision of computer time on the BP High Performance Computing facility in Houston, USA. The authors are grateful to Mary Jane Angelo, Keith Gray, David Lewis, and Rene Salmon (all of BP) for computing support, and to Kevin West (BP) for scientific discussions.

Notes and References

(1) Campana, M.; Teichert, A.; Clarke, S.; Steitz, R.; Webster, J. R. P.; Zarbakhsh, A. Surfactant Adsorption at the Metal-Oil Interface. *Langmuir* **2011**, *27*, 6085–6090.

(2) Lundgren, S. M.; Ruths, M.; Danerlöv, K.; Persson, K. Effects of unsaturation on film structure and friction of fatty acids in a model base oil. *J. Colloid Interface Sci.* **2008**, *326*, 530–536.

(3) Campen, S.; Green, J.; Lamb, G.; Atkinson, D.; Spikes, H. On the increase in Boundary Friction with Sliding Speed. *Tribol. Lett.* **2012**, *48*, 237–248.

(4) Ruths, M.; Lundgren, S.; Danerlov, K.; Persson, K. Friction of fatty acids in nanometer-sized contacts of different adhesive strength. *Langmuir* **2008**, *24*, 1509–1516.

(5) Zhang, L.; Chen, L.; Wan, H. Q.; Chen, J. M.; Zhou, H. D. Synthesis and tribological properties of stearic-acid-modified anatase (TiO_2) nanoparticles. *Tribol. Lett.* **2011**, *41*, 409–416.

(6) Qian, J. H.; Yin, X. Y.; Wang, N.; Liu, L.; Xing, J. J. Preparation and tribological properties of stearic acid-modified hierarchical anatase TiO_2 microcrystals. *Appl. Surf. Sci.* **2012**, *258*, 2778–2782.

(7) Wang, Y. H.; Wan, Y.; Wang, W. X.; Yang, S. Y. Friction-reducing properties of stearic acid modification of the Cu_2S film on the copper substrate. *J. Alloy. Compd.* **2013**, *557*, 179–183.

(8) Greenfield, M. L.; Ohtani, H. Molecular dynamics simulation study of model friction modifier additives confined between two surfaces. *Tribol. Lett.* **1999**, *7*, 137–145.

(9) Onodera, T.; Morita, Y.; Suzuki, A.; Koyama, M.; Tsuboi, H.; Hatakeyama, N.; Endou, A.; Takaba, H.; Kubo, M.; Dassenoy, F.; Minfray, C.; Joly-Pottuz, L.; Martin, J.-M.; Miyamoto, A. A Computational Chemistry Study on Friction of h-MoS_2. Part I. Mechanism of Single Sheet Lubrication. *J. Phys. Chem. B* **2009**, *113*, 16526–16536.

(10) Onodera, T.; Morita, Y.; Nagumo, R.; Miura, R.; Suzuki, A.; Tsuboi, H.; Hatakeyama, N.; Endou, A.; Takaba, H.; Dassenoy, F.; Minfray, C.; Joly-Pottuz, L.; Kubo, M.; Martin, J.-M.; Miyamoto, A. A Computational Chemistry Study on Friction of h-MoS_2 Part II Friction Anisotropy. *J. Phys. Chem. B* **2010**, *114*, 15832–15838.

(11) Sivebaek, I. M.; Samilov, V. N.; Persson, B. N. J. Velocity Dependence of Friction of Confined Hydrocarbons. *Langmuir* **2010**, *26*, 8721–8728.

(12) Sivebaek, I. M.; Samoilov, V. N.; Persson, B. N. J. Effective Viscosity of Confined Hydrocarbons. *Phys. Rev. Lett.* **2012**, *108*, 036102.

(13) Berro, H.; Fillot, N.; Vergne, P. Molecular dynamics simulation of surface energy and ZDDP effects on friction in nano-scale lubricated contacts. *Tribol. Int.* **2010**, *43*, 1811–1822.

(14) Mazyar, O. A.; Jennings, G. K.; McCabe, C. Frictional Dynamics of Alkylsilane Monolayers on SiO_2: Effect of 1-n-Butyl-3-methylimidazolium Nitrate as a Lubricant. *Langmuir* **2009**, *25*, 5103–5110.

(15) Lewis, J. B.; Vilt, S. G.; Rivera, J. L.; Jennings, G. K.; McCabe, C. Frictional Properties of Mixed Fluorocarbon/Hydrocarbon Silane Monolayers: A Simulation Study. *Langmuir* **2012**, *28*, 14218–14226.

(16) Rivera, J. L.; Jennings, G. K.; McCabe, C. Examining the frictional forces between mixed hydrophobic âĂŞ hydrophilic alkylsilane monolayers. *J. Chem. Phys.* **2012**, *136*, 244701.

(17) Thompson, P. A.; Robbins, M. O. Shear-flow near solids - epitaxial order and flow boundary-conditions. *Phys. Rev. A* **1990**, *41*, 6830–6837.

(18) He, G.; Müser, M. H.; Robbins, M. O. Adsorbed Layers and the Origin of Static Friction. *Science* **1999**, *284*, 1650–1652.

(19) He, G.; Robbins, M. O. Simulations of the kinetic friction due to adsorbed surface layers. *Tribol. Lett.* **2001**, *10*, 7–14.

(20) He, G.; Robbins, M. O. Simulations of the static friction due to adsorbed molecules. *Phys. Rev. B* **2001**, *64*, 035413.

(21) Müser, M. H.; Wenning, L.; Robbins, M. O. Simple microscopic theory of Amontons's laws for static friction. *Phys. Rev. Lett.* **2001**, *86*, 1295–1298.

(22) Barsky, S.; Robbins, M. O. Bulk and interfacial shear thinning of immiscible polymers. *Phys. Rev. E* **2002**, *65*, 021808.

(23) Müser, M. H.; Urbakh, M.; Robbins, M. O. Statistical mechanics of static and low-velocity kinetic friction. *Adv. Chem. Phys.* **2003**, *126*, 187–272.

(24) Bitsanis, I. A.; Pan, C. The origin of "glassy" dynamics at solid-oligomer interfaces. *J. Chem. Phys.* **1993**, *99*, 5520–5527.

(25) Manias, E.; Hadziioannou, G.; Tenbrinke, G. Effect of shear on the desorption of oligomers in nanoscopically confined fluids. *J. Chem. Phys.* **1994**, *101*, 1721–1724.

(26) Hirz, S.; Subbotin, A.; Frank, C.; Hadziioannou, G. Static and kinetic friction of strongly confined polymer films under shear. *Macromolecules* **1996**, *29*, 3970–3974.

(27) Gao, J.; Luedtke, W. D.; Landman, U. Friction Control in Thin-Film Lubrication. *J. Phys. Chem. B* **1998**, *102*, 5033–5037.

(28) Gao, J.; Luedtke, W. D.; Gourdon, D.; Ruths, M.; Israelachvili, J. N.; Landman, U. Frictional Forces and Amontons' Law: From the Molecular to the Macroscopic Scale. *J. Phys. Chem. B* **2004**, *108*, 3410–3425.

(29) Sivebaek, I. M.; Samoilov, V. N.; Persson, B. N. J. Frictional properties of confined polymers. *Euro. Phys. J. E* **2008**, *27*, 37–46.

(30) Martini, A.; Hsu, H.-Y.; Patankar, N. A.; Lichter, S. Slip at High Shear Rates. *Phys. Rev. Lett.* **2008**, *100*, 206001.

(31) Martini, A.; Dong, Y.; Perez, D.; Voter, A. F. Low-Speed Atomistic Simulation of Stick-Slip Friction using Parallel Replica Dynamics. *Tribol. Lett.* **2009**, *36*, 63–68.

(32) Farrow, M. R.; Chremos, A.; Camp, P. J.; Harris, S. G.; Watts, R. F. Molecular simulations of friction modification in nanoscale fluid layers. *Tribol. Lett.* **2011**, *42*, 325–337.

(33) Dai, L.; Minn, M.; Satyanarayana, N.; Sinha, S. K.; Tan, V. B. C. Identifying the Mechanisms of Polymer Friction through Molecular Dynamics Simulation. *Langmuir* **2011**, *27*, 14861–14867.

(34) Carrillo, J.-M. Y.; Russano, D.; Dobrynin, A. V. Friction between Brush Layers of Charged and Neutral Bottle-Brush Macromolecules. Molecular Dynamics Simulations. *Langmuir* **2011**, *27*, 14599–14608.

(35) Carrillo, J.-M. Y.; Brown, W. M.; Dobrynin, A. V. Explicit Solvent Simulations of Friction between Brush Layers of Charged and Neutral Bottle-Brush Macromolecules. *Macromolecules* **2012**, *45*, 8880–8891.

(36) Priezjev, N. V. Interfacial friction between semiflexible polymers and crystalline surfaces. *J. Chem. Phys.* **2012**, *136*, 224702.

(37) Goujon, F.; Ghoufi, A.; Malfreyt, P.; Tildesley, D. J. Frictional forces in polyelectrolyte brushes: effects of sliding velocity, solvent quality and salt. *Soft Matter* **2012**, *8*, 4635–4644.

(38) Goujon, F.; Ghoufi, A.; Malfreyt, P.; Tildesley, D. J. The kinetic friction coefficient of neutral and charged polymer brushes. *Soft Matter* **2013**, *9*, 2966–2972.

(39) Elliott, I. G.; Kuhl, T. L.; Faller, R. A Molecular Dynamics Technique to Extract Forces in Soft Matter Systems Under Compression With Constant Solvent Chemical Potential. *J. Chem. Theory Comput.* **2012**, *8*, 1072–1077.

(40) Hoang, H.; Galliero, G. Shear behavior of a confined thin film: Influence of the molecular dynamics scheme employed. *J. Chem. Phys.* **2013**, *138*, 054707.

(41) Wood, M. H.; Clarke, S. M.; Casford, M. T.; Zarbaksh, A.; Welbourn, R. J. L.; Charlton, T. Amine adsorption at the iron oxide-oil interface. **2013**, submitted.

(42) Doig, M.; Camp, P. J. The structures of hexadecylamine films adsorbed on iron-oxide surfaces in dodecane and hexadecane. **2013**, in preparation.

(43) Plimpton, S. J. Fast Parallel Algorithms for Short-Range Molecular Dynamics. *J. Comp. Phys.* **1995**, *117*, 1–19.

(44) LAMMPS Molecular Dynamics Simulator. http://lammps.sandia.gov.

(45) Blake, R. L.; Hessevick, R. E.; Zoltai, T.; Finger, L. W. Refinement of the hematite structure. *Am. Mineral.* **1966**, *51*, 123–129.

(46) Humphrey, W.; Dalke, A.; Schulten, K. VMD – Visual Molecular Dynamics. *J. Mol. Graphics* **1996**, *14*, 33–38.

(47) Mayo, S. L.; Olafson, B. D.; Goddard III, W. A. DREIDING: a generic force field for molecular simulations. *J. Phys. Chem.* **1990**, *94*, 8897–8909.

(48) Frisch, M. J.; Trucks, G. W.; Schlegel, H. B.; Scuseria, G. E.; Robb, M. A.; Cheeseman, J. R.; Montgomery, J. A., Jr.; Vreven, T.; Kudin, K. N.; Burant, J. C.; Millam, J. M.; Iyengar, S. S.; Tomasi, J.; Barone, V.; Mennucci, B.; Cossi, M.; Scalmani, G.; Rega, N.; Petersson, G. A.; Nakatsuji, H.; Hada, M.; Ehara, M.; Toyota, K.; Fukuda, R.; Hasegawa, J.; Ishida, M.; Nakajima, T.; Honda, Y.; Kitao, O.; Nakai, H.; Klene, M.; Li, X.; Knox, J. E.; Hratchian, H. P.; Cross, J. B.; Bakken, V.; Adamo, C.; Jaramillo, J.; Gomperts, R.; Stratmann, R. E.; Yazyev, O.; Austin, A. J.; Cammi, R.; Pomelli, C.; Ochterski, J. W.; Ayala, P. Y.; Morokuma, K.; Voth, G. A.; Salvador, P.; Dannenberg, J. J.; Zakrzewski, V. G.; Dapprich, S.; Daniels, A. D.; Strain, M. C.; Farkas, O.; Malick, D. K.; Rabuck, A. D.; Raghavachari, K.; Foresman, J. B.; Ortiz, J. V.; Cui, Q.; Baboul, A. G.; Clifford, S.; Cioslowski, J.; Stefanov, B. B.; Liu, G.; Liashenko, A.; Piskorz, P.; Komaromi, I.; Martin, R. L.; Fox, D. J.;

Keith, T.; Al-Laham, M. A.; Peng, C. Y.; Nanayakkara, A.; Challacombe, M.; Gill, P. M. W.; Johnson, B.; Chen, W.; Wong, M. W.; Gonzalez, C.; Pople, J. A. Gaussian 03. 2004; Gaussian, Inc., Wallingford, CT.

(49) The choices of T and P correspond to typical physical conditions of some critical areas of combustion engines. A systematic survey of structure and friction at other temperatures and pressures has been carried out, but the current choices are representative.

(50) Allen, M. P.; Tildesley, D. J. *Computer simulation of liquids*; Clarendon Press: Oxford, 1987.

(51) Dorinson, A. The Slow-Speed Frictional Behaviour of Some Lubricant Additive Type-Substances. *ASLE Trans.* **1970**, *13*, 215–224.

(52) Dieterich, J. H. Modeling of rock friction .1. Experimental results and constitutive equations. *J. Geophys. Res.* **1979**, *84*, 2161–2168.

(53) Dieterich, J. H. Modeling of rock friction .2. Simulation of pre-seismic slip. *J. Geophys. Res.* **1979**, *84*, 2169–2175.

(54) Ruina, A. Slip instability and state variable friction laws. *J. Geophys. Res.* **1983**, *88*, 359–370.

(55) Gu, J. C.; Rice, J. R.; Ruina, A. L.; Tse, S. T. Slip motion and stability of a single degree of freedom elastic system with rate and state dependent friction. *J. Mech. Phys. Sol.* **1984**, *32*, 167–196.

(56) Briscoe, B. J.; Evans, D. C. B. The shear properties of Langmuir-Blodgett layers. *Proc. Roy. Soc. Lond. A* **1982**, *380*, 389–407.

(57) Perez, D.; Dong, Y.; Martini, A.; Voter, A. F. Rate theory description of atomic stick-slip friction. *Phys. Rev. B* **2010**, *81*, 24515.

(58) Eyring, H. Viscosity, Plasticity, and Diffusion as Examples of Absolute Reaction Rates. *J. Chem. Phys.* **1936**, *4*, 283–291.

(59) Gupta, S. A.; Cochran, H. D.; Cummings, P. T. Shear behavior of squalane and tetracosane under extreme confinement. III. Effect of confinement and viscosity. *J. Chem. Phys.* **1997**, *107*, 10335–10343.

(60) Bair, S.; McCabe, C.; Cummings, P. T. Comparison of Nonequilibrium Molecular Dynamics with Experimental Measurements in the Nonlinear Shear-Thinning Regime. *Phys. Rev. Lett.* **2002**, *88*, 058302.

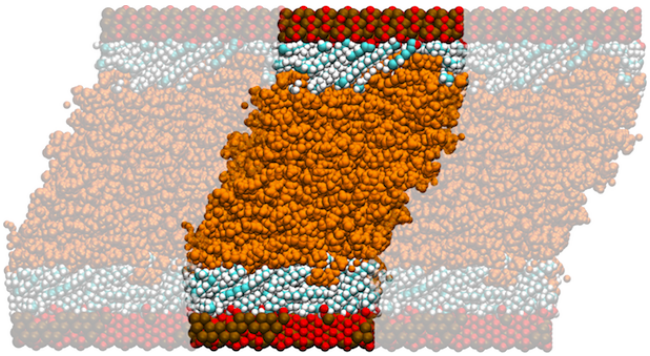

For Table of Contents Only